(12)

Final Report
Contract No.: ONR N00014-88-K-0317
(ONR N00014-92-J-1868)

Properties of E-beam Interactive Oxide Films for Nanometer Scale Structures

by

R. C. Buchanan*
J. L. Hollenbeck
J. Kim*

October 1993

Department of Materials Science and Engineering
Ceramic Division
University of Illinois at Urbana-Champaign
105 S. Goodwin Ave.
Urbana, IL 61801

This research was supported by DARPA under
Office of Naval Research Sponsorship

*Current Address Univ. of Cincinnati, 498 Rhodes Hall, Cincinnati, OH 45221

SECURITY CLASSIFICATION OF THIS PAGE

REPORT DOCUMENTATION PAGE

1a. REPORT SECURITY CLASSIFICATION
Unclassified

1b. RESTRICTIVE MARKING

2a. SECURITY CLASSIFICATION AUTHORITY

2b. DECLASSIFICATION/DOWNGRADING SCHEDULE

3. DISTRIBUTION/AVAILABILITY OF REPORT Widespread; required # of copies to defense documentation ctr. individuals and organizations on approved distribution list furnished by Metallurgy & Cer. Pro

4. PERFORMING ORGANIZATION REPORT NUMBER(S)
Report # 19

5. MONITORING ORGANIZATION

6a. NAME OF PERFORMING ORGANIZATION SYMBOL
University of Illinois

6b. OFFICE (if applicable)

7a. NAME OF MONITORING ORGANIZATION

6c. ADDRESS(City, State and ZIP Code)
Department of Materials Science & Engineering
105 S. Goodwin, Urbana, IL 61801

7b. ADDRESS(City, State and ZIP Code)

8a. NAME OF FUNDING/SPONSORING ORGANIZATION
DARPA
Office of Naval Research

8b. OFFICE (if applicable)

9. PROCUREMENT INSTRUMENT IDENTIFICATION NUMBER

8c. ADDRESS (City, State and ZIP code)
Division of Materials Research Arlington, VA 22217

10. SOURCE OF FUNDING NOS.

PROGRAM ELEMENT NO.	PROJECT NO.	TASK NO.	WORK UNIT NO

11. TITLE (include Security Classification)
Properties of E-beam Interactive Oxide Films for Nanometer Scale Structures

12. PERSONAL AUTHOR(S)
R. C. Buchanan, J. L. Hollenbeck and J. Kim

13a. TYPE OF REPORT
Final

13b. TIME COVERED
FROM 10/1/88 TO 12/1/93

14. DATE OF REPORT(Yr.,Mo.,Day)
Nov. 5 , 1993

15. PAGE COUNT
37

16. SUPPLEMENTARY NOTATION
E-beam lithography

17. COSATI CODES

FIELD	GROUP	SUB. GR.

18. SUBJECT TERMS (continue on reverse if necessary and identify by block number)
Lithography, Nanostructure, Oxide, E-beam, Memory

19. ABSTRACT (Continue on reverse if necessary and identify by block number)

SEE NEXT PAGE

20. DISTRIBUTION/AVAILABILITY OF ABSTRACT
UNCLASSIFIED UNLIMITED SAME AS RPT DTIC USERS

21. ABSTRACT SECURITY CLASSIFICATION
Unclassified

22a. NAME OF RESPONSIBLE INDIVIDUAL

22b. TELEPHONE NUMBER (include Area Code)

22c. OFFICE SYMBOL

DD FORM 1473, 83 APR

results in a measurable improvement in film sensitivity. These effect are

Abstract

E-beam generated ultrastructures on oxide film substrates have been investigated for high density memory and lithographic applications. In order to create the nanometer scale patterns (holes, lines, channels), a dedicated STEM have been used and also used for exposure studies, imaging, microdiffraction analysis and monitoring the transmitted beam studies. Amorphous films of Al_2O_3, Y_2O_3, Sc_2O_3, $3Al_2O_3{\cdot}2SiO_2$, and $MgO{\cdot}Al_2O_3$ are deposited on to substrate at cryogenic temperature. Amorphous film structure is necessary to achieve rapid removal of material during e-beam exposure. Hole resolution in the sputtered oxide films of 5 nm holes on 8.1 nm centers was achieved with exposure times in the millisecond range, 2 ~ 3 orders of magnitude lower than produced by other technique. Deposition parameters and film thickness have been studied. The gas ambient on thin films electron dose are strongly related to the drilling speed. A possible mechanism for the exposure process is also developed.

Table of Contents

Properties of E-beam Interactive Oxide Films for Nanometer Scale Structures

R. C. Buchanan
Dept. of Material Science and Engineering
University of Illinois , Urbana, IL 61801

I. Introduction

The demands of high density memory system and nanoscale lithographic technology have been increased during the last decade. The barrier is that there is no suitable material to obtain this high spatial resolution. The selective removal of material in highly ionic solids was first observed in NaCl foils by Broers in 1978[1]. A number of oxide and metal halide compounds when exposed to high intensity electron beam irradiation undergo a rapid loss of constituents permitting lithographic features to be produced on the order of 1~ 20 nm[2, 3]. Structures on this scale are among the smallest currently obtainable in lithographic systems, surpassing the limit imposed by the spatial range of secondary electrons generated in conventional high resolution polymeric materials, such as PMMA[4]. The inherent high resolution characteristics of these materials, as well as a lack of understanding of the exposure process involved, has fueled an interest in further study of inorganic resist materials.

Fabrication of nanometer scale structures has wide ranging application in such fields as microelectronics, molecular biology and experimental physics. Two applications where ablative inorganic resist materials have been examined include high resolution resist for lithography and high density storage media for electron beam addressing memory systems[5]. Substrate characteristics desirable in the above applications, in addition to nanometer scale resolution, include low dosage requirements for exposure, high material removal rates, high contrast, good physical and chemical durability and good thermal conductivity.

To date the majority of studies reported on high resolution inorganic resists concentrated on metal halides. In these materials, material loss strongly depends on composition. In addition, the lithographic characteristics of oxide materials have been observed by Hollenbeck and Buchanan [6, 7] to depend on the method of film preparation and on the resulting microstructural characteristics. The latter studies have shown that proper control of film deposition should produce improvements in resist properties, particularly exposure requirements.

It is the purpose of this research to develop new oxide resist materials capable of nanoscale resolution and to determine the interrelationships between the various parameters of a lithographic system. The results show that film characters are sensitive to the exposure of rf sputtered films included amorphous film structure , inert gas concentration, ionic character, heat of formation, and film thickness. The dose rate and energy of the incident beam were also found to influence the does requirement for exposure. The most sensitive films were found to be Al_2O_3, Y_2O_3, Sc_2O_3, $3Al_2O_3 \cdot 2SiO_2$, and $MgO \cdot Al_2O_3$ which required an exposure dose of approximately 5×10^3 C/cm^2. The ultimate resolution in amorphous Al_2O_3 films consisted of 5.0 nm holes on 8.9 nm centers. The exposure process was modeled as a sequence of events beginning with desorption of surface oxygen and generation of bulk defects, as followed by extensive surface desorption, diffusion of bulk defects and rapid expulsion of components remaining in the irradiated volume.

II. Experimental Procedure

The oxide films were deposited by rf sputtering from dense polycrystalline oxide tagets directly onto formvar coated 200 mesh grids stabilized with SiO. The resulting resist/substrate arrangement is shown in figure 1. The formvar and SiO coatings are amorphous and show no deterioration under exposure conditions. Sputtering parameters were chosen to allow the fabrication of both polycrystalline and amorphous films from 15 ~ 150 nm in thickness. To promote the formation of amorphous films, the substrate temperature was controlled at 77 K through the use of a liquid nitrogen cold stage.

Electron beam exposure of the thin oxide films was carried out using a modified V. G. Microscope HB-5 STEM, capable of producing a 100 keV beam of electrons with a dose rate of 1×10^5 A/cm^2 and a final spot diameter less than 1 nm. Generation of lithographic patterns is being carried out through computer control of the beam deflection and beam blanking systems in the microscope.

Structural and chemical chraterization was primary done by a Philips EM400T equipped with EDS and RBS. The RBS analysis was carried out using incident 1 MeV He^+ and was performed on samples deposited on polished Si wafers. The microdiffraction capability of the V. G. HB-5 allowed electron diffraction analysis to be performed on individual crystallites as small as the beam spot size(1 nm) when operating the microscope in spot mode. This permitted analysis of local structural and crystallographic changes accompanying the formation of nanometer scale features. Digital image enhancement features of the system were used in anlyzing diffraction data.

III. Results and Discussion

The two most important deposition parameters found to influence the microstructure of rf sputtered oxide films were substrate temperature and rf power. Deposition conditions necessary to promote the formation of uniform amorphous films were also found to be strongly dependent on the material itself. Using a substrate temperature of 77 K amorphous film structure was produced in seven of the eight oxides studied. The deposition of films at cryogenic temperature limited diffusion of adatoms on growing films and resulted almost exclusively in amorphous film structures. Limited sputtering power minimized local heating of the film surface during deposition. To avoid local surface heating in films, powers were limited to less than 50 Watts and a 10 min cooling period for every 30 min of deposition time. Bright field TEM images of polycrystalline and amorphous Al_2O_3 films along with their corresponding SAD patterns and X-ray spectra are shown in figure 2. RBS data from a series of amorphous Al_2O_3 films was used to establish quantitative standards and to confirm the Ar concentrations determined by X-ray analysis. Ar concentration measured by X-ray and RBS analysis in a series of three films were found to agree with ±0.1% atomic %. SIMS spectra used to determine the Ar concentration changes were checked. The Ar concentration was found to not fluctuate in whole films. These data are shown in figure 3. The amorphous films showed good uniformity, good density, very little contrast and a characteristic diffuse diffraction pattern. X-ray spectra shows that the relative intensity of Ar peaks is different between polycrystalline and amorphous films. The Ar concentration was found to range from approximately 1.7 ~ 3.1 at% in amorphous films depend on deposition condition. The summary of rf sputtered films structures is shown in table 1.

The initial response of rf sputtered oxide films under E-beam dose rate of approximately 1×10^5 A/cm^2. Polycrystalline oxide films showed no mass loss or lithographic response under extended periods (>10 s) of irradiation. Amorphous films were found to exhibit lithographic characteristics with the dose required for exposure varying from approximately 1×10^5 A/cm^2 (~50 ms) in the most sensitive materials. The initial response of e-beam dose is summarized in table 2. It becomes clear from the data in table 2 that removal of material under exposure conditions is strongly dependent on both film structure and composition. Examples of lithographic structures which can be produced in the six oxides showing nanometer scale lithographic characteristics are shown in figure 4 (A) and (B). These structures include both holes, which are actually columns in 3-dimensions, and lines, which are troughs in 3-dimension.

The dose requirement of rf sputtered films of Al_2O_3, Y_2O_3, Sc_2O_3, $3Al_2O_3 \cdot 2SiO_2$, and $MgO \cdot Al_2O_3$ have also been found to show a response which is two or three orders of magnitude more sensitive than oxides produced by such techniques as anodization[5], collection of smoke particles[8] or crushing of powders[9]. Although films prepared by other techniques have not been well characterized, one obvious chemical difference in the rf sputtered films is the presence of inert gas. The large increase in sensitivity observed in rf sputtered films indicates that inert gas incorporated into the film structure may, at least in part, be responsible for improved sensitivity.

A summary of selected material properties of the single metal oxides examined is given in table 3. Material properties which were found to correlate well with the exposure response of amorphous oxide films were the bonding character, heat of formation and melting point. A rapid response was found to occur in materials with high ionic character, high heats of formation and high melting points. The highly ionic materials with high bonding strength are required to produce films with sufficient sensitivity to make them viable resists.

The process of material removal which occurs during the exposure of a single hole in amorphous Al_2O_3 was studied using multiple dose / multiple spacing test pattern and monitoring of transmitted beam signal. Figure 5 shows a STEM bright field image of a test pattern generated using four different total doses, or exposure times and four different hole spacings. Also shown in figure 5 is the hole diameter produced as a function of exposure time and a trace of the transmitted beam signal for the consecutive holes in amorphous Al_2O_3. From the bright field image and a plot of hole size vs. total dose it was found that small incomplete holes were produced during initial exposure and that these holes continued to increase in diameter upon further exposure. This increase in hole size continued until a diameter of approximately 10.6 nm was reached.

Direct evidence that atomic displacement occurs over the range of many atomic spacings during exposure was observed both in the redeposition of material into fully developed closely spaced hole and line structures, and in the formation of small crystallites at the edges of newly formed structures. Figure 6 shows two conditions under which material was found to be redeposited in previously exposed areas: (A) when the e-beam was scanned over relatively small area and (B) when line or hole patterns intersect or are spaced very close together. (A) shows a pattern produced in amorphous Al_2O_3 in which a portion of the pattern has been observed at higher magnification under normal bright field scanning conditions. This area of the pattern shows that the diameter of existing holes was reduced from redepostion of material into them and the entire area appears brighter due to loss of material in the previously unexposed regions between holes. In (B) the vertical series of lines initially produced in amorphous $3Al_2O_3 \cdot 2SiO_2$ were found to be refilled by subsequently exposed horizontal lines. Refilled regions are most easily seen in segments of the vertical lines between the horizontal lines.

The formation of small crystallites was observed in STEM bright field images after the exposure of many different patterns. Microdiffraction patterns produced from similar crystallites, formed both near newly exposed patterns and at hole and line edges, are shown in figure 7. The three microdiffraction patterns were taken from amorphous films of Al_2O_3, Y_2O_3 and ZrO_2 and were found to correspond to Al, Y, Zr patterns respectively. The metal constituents in the irradiated volume of the film thus appear to be spatially separated from the lattice oxygens during exposure and were reduced to the metallic state.

From the evidence above e ablative removal of material under e-beam exposure appears to occur through a multiple step sequence of events starting with desorption of surface oxygen and finishing with the rapid displacement of bulk cation, oxygen and inert gas film components in the irradiated volume. Figure 8 schematically illustrates the progression of hole development believed to occur in oxide films beginning with: (A) the desorption of oxygen from the surface and generation of defects in the bulk, (B) and (C) continued surface desorption, (D) rapid expulsion of components remaining in the irradiated volume and (E) and (F) the resulting hole which retains metallic species at hole edges and which increases in size with continued exposure.

The desorption of oxygen from surfaces and generation of bulk defects in oxide films is believed to occur simultaneously as a result of electronic excitations produced by inelastic scattering of incident e-beam. One model which is useful in describing desorption and defect generation in oxides is the ESD theory[10-12]. In this model, charge transfer in highly ionic maximal valence oxides occurs through an Auger decay process and can result in both the loss of surface oxygen or displacement of bulk oxygen atoms from their original electrostatic equilibrium position in the structure. The generation of bulk oxygen and metal defects can be described by the defect equations below.

$$3O_0 = 3/2\ O_2 + 3V_O + 6e$$

$$2Al_{Al} + 6e = 2Al_{metal}$$

Once bulk defects are formed a preferential diffusion of cations away from the irradiated volume appears to occur. Evidence of the separation and preferential diffusion of cations is found in the presence of reduced metallic regions at hole edges. Electric field during e-beam exposure can assist the movement of cations away from the immediate area and also hinder any diffusion of negatively charged oxygen species remaining. Although no direct evidence exists that oxygen and argon are the primary species in the irradiated volume, when the remaining material is rapidly displaced, the lack of any oxygen or inert gas re naining after exposure strongly support this. Using EELS, molecular oxygen peaks was reported to appear upon initial exposure, which then disappear upon completion of the structure[13].

It is still not clear what process may be controlling the final rapid removal of material under irradiation, however, it is safe to assume that this material must be in a highly defect and disordered state due to irradiation damage. The produced oxygen and remaining volume may combine to form molecular oxygen and the inert gas may coalesce to form bubbles. The volume expansion of gases formed in such a manner could be significant , producing a region of high pressure, and result in a rapid expulsion of material consistent with observation. Although no macroscopic evidence of heating was observed, local heating from the relatively short duration high intensity exposure could result in brief rapid expansion of material, in solid or gaseous form, thereby generating a pressure capable of expelling material from the hole. It is quite clear, however, that some critical point is reached, or a critical volume of material is formed, which is associated with the final rapid removal of material and formation of a complete hole.

The contrast response of polycrystalline and amorphous rf sputtered films cannot be explained simply in terms of the initial damage mechanism but rather indicates that microstructural characteristics are also extremely important to the overall speed of the exposure process. Deposition of oxide films at cryogenic temperature has produced structures which are not stable at room temperature. This instability may help drive atomic rearrangement. The relatively open structure of amorphous films is also believed to significantly enhance the rate of bulk atomic diffusion. The greatly reduced dose requirements of rf sputtered films relative to those produced by other techniques is also strong evidence that both microstructural and chemical characteristics strongly influence the rate at which material can be removed. From the qualitative exposure model proposed above the total exposure time or dose requirement of a given oxide resist should be dependent on the rate at which surface species desorb and bulk defects can diffuse and finally be displaced or expelled from the irradiated volume.

The parameters, such as film thickness, exposure parameters and inert gas incorporation, which were found to primarily influence the dose requirement in a given material are discussed below. Thickness of the oxide films was found to strongly affect the exposure dose requirement. Figure 6 shows the end point dose measured as a function of Al_2O_3 film thickness between approximately 15 and 150 nm. At film thickness greater than approximately 100 nm it was found that the dose requirement begins to increase, such that an optimum thickness occurs at 90 nm, where the film is most sensitive. The contrast, reported as the percent change in transmitted beam signal after exposure is also plotted in figure 9. This parameter is important in data storage applications and over this thickness range should be approximately proportional to film thickness, as observed. The influence of film thickness on dose requirement is believed to involve the removal of oxygen and inert gas remaining in the developing hole. If the film is very thin, oxygen can be removed predominantly through surface desorption and the critical volume and inert gas required for rapid expulsion may never be generated. In very thick films (>100 nm) the larger amount of material which must be removed and increased scattering of the incident electrons, appear to result in a slower rate of final structure formation.

Two exposure parameters which can be strongly influence e-beam film interactions are the dose rate and beam energy. The effect which dose rate and beam energy had on the time and corresponding end dose required for exposure of a single hole in an 87.5 nm thick Al_2O_3 film is shown in figure 10. The decrease in exposure time with increasing dose rate covered approximately an order of magnitude between dose rates of 5×10^2 and 1×10^5 A/cm^2. This decrease appears to result straightforwardly from the increased number of electrons incident on the sample in a given time at higher dose rates. However, the end point dose also increased as the dose rate increased. This indicates that the total number of incident electrons required to complete the exposure of a single hole increased as the rate at which electrons impinge on the sample increases. In terms of the exposure model developed, the probability for surface desorption and defect generation should not be dependent on dose rate. Therefore, the rate at which these events occur should increase proportionately with dose rate. The bulk diffusion processes which control the speed of material displacement in the bulk irradiated volume should, however, be relatively independent of dose rate over this range. Since there appears to be a critical volume of oxygen and inert gas associated with the final removal of material and the completion of exposure, the attainment of this critical condition will ultimately be controlled by the time required for sufficient material diffusion to occur. As a result, the diffusion of material within the bulk of irradiated film is believed to be the rate controlling step in the exposure process. The increase of beam energy, while not as significant as that of dose rate, does produce a factor of two improvement in sensitivity at the higher accelerating potentials.

To isolate the effect of inert gas incorporation on the exposure characteristics of the oxide films a series of 90 nm thick amorphous Al_2O_3 films containing various amounts of Ar were examined. These films were deposited using different Ar pressure. These Ar concentration in the films are given Table 4 and the Ar concentration increased as sputtering pressure was decreased. In addition to Ar concentration, amorphous films produced using a Kr atmosphere and incorporating Kr in the structure was also examined. Figure 11 shows the end point dose and time required for complete exposure of amorphous Al_2O_3 films as a function of Ar concentration. The increment of Ar concentration resulted in huge improvement of film sensitivity. Figure 12 shows the improvement in film sensitivity using Kr. Kr, which has a larger atomic size compared to Ar, results in a measurable improvement in film sensitivity. These effect are strongly related to the more open structure of amorphous films.

The resolution of hole and line patterns was studied as a function of film thickness and total exposure dose, using multiple dose / multiple spacing patterns. Table 5 and figure 13 shows these effects. Optimum film thickness was again found to occur at approximately 90 nm where 5.0 nm holes could produced on 8.9 nm centers. Slightly better resolution is reported at exposure doses of 13×10^2 and 4×10^2 C/cm^2, however, holes formed at these doses did not result in complete material removal.

A number of factors are believed to contribute the final diameter of holes produced in rf sputtered oxide films, including the spatial distribution of electrons in the beam, divergence of the beam, noise in the exposure system and the range of inelastic scattering events. The most significant contribution is believed to be the noise in the exposure system which produces variation in the beam position. Noise is not unusual in electron beam systems and can arise from a number of sources, including external mechanical, acoustic and magnetic sources, as well as from electrical and mechanical instabilities in the system itself[14]. Contributions from beam divergence and the spatial distribution of electrons in the beam will also contribute to exposure of material outside the nominal 1 nm diameter of the incident beam but cannot alone account for the 5.0 nm diameter hole produced in the optimized amorphous film. The range of inelastic scattering events themselves should under ideal exposure conditions be the resolution limiting mechanism[15].

Conclusively, amorphous film structure was found to be a requirement for rapid material removal to occur while material properties found to influence irradiation response include ionic character, heat of formation and melting point. The specific role of the material properties are not clear but may involve the film growth processes and variations in final structure. As a result of observation made, a format for predicting the response in new oxide materials has now been established. Improvement in the lithographic characteristics of high resolution oxide resists have been shown to be possible through improved understanding of the exposure process. Figure 14 shows also the possibility of applying this technique to other applications, such as memory systems. This improved understanding, along with the development of new materials, is expected to result in more widespread application of these materials as the need for nanometer scale lithography techniques continues to grow.

IV. Conclusions

1. A number of e-beam interactive high resolution oxide resist materials have been developed, including Al_2O_3, Y_2O_3, Sc_2O_3, $3Al_2O_3{\cdot}2SiO_2$, and $MgO{\cdot}Al_2O_3$. These resists , produced by rf sputtering at cryogenic temperature, can be exposed much more rapidly and with a lower dose than materials prepared by other techniques.
2. The incorporation of Ar in amorphous Al_2O_3 was found to decrease the end point dose requirement, as the Ar concentration increased. Incorporation of Kr at the same concentration was found to further decrease the end point dose requirement.
3. High ionic character, high heat of formation and high melting point were identified as desirable material characteristics.
4. A qualitative model of the exposure process has been developed. The process was modeled as a sequence of events beginning with the desorption of oxygen from the film surface and generation of bulk defects. Further surface

desorption and the diffusion of bulk defects is followed by a rapid expulsion of components remaining in the irradiated volume. Initial desorption and defect generation is believed to result from electronic excitations produced by inelastic scattering.

5. Film thickness was found to have a significant effect on the end point dose requirements. The best result was obtained at approximately 90 nm. No threshold current densities were observed in any of the films examined under dose rates as low as 1×10^{3} C/cm^{2}.

6. The high resolution of amorphous Al_2O_3 films allowed the production of 5.0 nm holes on 8.9 nm centers and 8.0 nm lines on 12.0 nm centers. Noise in the exposure system was believed to limit the ultimate resolution.

V. Acknowledgments

We thank the staffs of Materials Research Labs for the use of the equipment pertaining to this experiment. This work was supported by DARPA under Office of Naval Research contracts No. N00014-88-K-0317 and N0014-92-J-1868.

VI. Reference

1. A. N. Broers J. Cuomo J. Harper W. Molzen R. Laibowitz and M. Pomerants, "High Resolution Electron Beam Fabrication Using STEM," *9th International Congress on Electron Microscopy*, III 343-354 (1978).

2. D. C. Joy, "The Spatial Resolution Limit of Electron Lithography," *Microelectronic Eng.*, 1 103-19 (1983).

3. E. Kratschmer and M. Issacson, "Nanostructure Fabrication in Metals, Insulators, and Semiconductors Using Self-Developing Metal Inorganic Resists," *J. Vac. Sci. Technol.*, B4 361-4 (1986).

4. M. Issacson and A. Murray, "In Situ Vaporization of Very Low Molecular Weight Resists Using 1/2 nm Diameter Electron Beams," *J. Vac. Sci. Technol*, 19 [4] 1117-20 (1981).

5. M. E. Mochel J. A. Eades M. Metzger J. I. Meyer and J. M. Mochel, "Electron Beam Cutting in Amorphous Alumina Sheets," *Appl. Phys. Lett.*, 44 [5] 502-5 (1984).

6. J. L. Hollenbeck and R. C. Buchanan, "Properties of E-Beam Interactive Oxide Films," *Mat. Res. Soc. Symp.*, 72 289-294 (1986).

7. J. L. Hollenbeck and R. C. Buchanan, "Nanometer-Scale Structures Produced in Oxide Films," *Proceedings of the 45th Annual Meeting of the Electron Microscopy Society of America*, 396-7 (1987).

8. I. G. Salisbury, R. S. Timsit, S. D. Berger, and C. J. Humphreys, "Nanometer Scale Electron Beam Lithography in Inorganic Materials," *Appl. Phys. Lett.*, 45 [12] 1289-91 (1985).

9. S. D. Berger, J. M. Macaulay, and L. M. Brown, "Radiation Damage in TiOx at High Current Density," *Phil. Mag. Lett.*, 56 [5] 179-85 (1987).

10. M. L. Knotek and P. J. Fiebleman, "Stability of Ionically Bonded Surfaces in Ionizing Environments," *Surface Science*, 90 [78-90] (1979).

11. M. L. Knotek, "Radiation Induced Surface Decomposition," *Proceedings of the 41st Annual Meeting of Electron Microscopy Society of America*, 368-9 (1983).

12. M. L. Knotek, "Stimulated Desorption," *Rev. Prog. Phys.*, 47 1499-1561 (1984).

13. S. D. Berger I. G. Salisbury R. H. Milne D. Imeson and C. J. Humphreys, "Electron Energy-Loss Spectroscopy Studies of Nanometer -Scale Structures in Alumina Produced by Intense Electron-Beam Irradiation," *Phil. Mag. B*, 55 [3] 341-358 (1987).

14. E. Kratschmer, S. A. Rishton, D. P. Kern, and T. H. P. Chang, "Quantitative Analysis of Resolution and Instability in Nanometer Electron Beam Lithography," *J. Vac. Sci. Technol.*, B6 [6] 2074-79 (1988).

15. M. Isaacson and J. P. Langmore, "Determination of the Non-Localization of Inelastic Scattering of Electrons by Electron Microscopy," *Optik*, 41 [1] 92-6 (1974).

VII. List of Figures

Figure 8. Schematic illustration of material removal process in oxide resists: (A) desorption of surface oxygen and creation of bulk defects, (B) and (C) further surface desorption and defect generation, (D) rapid loss of remaining constituents, (E) Completed hole with metallic species remaining behind and (F) continued increase in hole diameter.

Figure 9. End point dose and contrast measures as a function of film thickness for amorphous Al_2O_3 films.

Figure 10. The effect of dose rate and accelerating potential on the (A) time and (B) end point dose required to expose an 87.5 nm thick amorphous Al_2O_3 film.

Figure 11. End point dose and exposure time required to expose 90 nm thick amorphous Al_2O_3 film as a function of Ar concentration (dose rate : 1.08×10^5 A/cm^2).

Figure 12. End point dose as a function of film thickness for amorphous Al_2O_3 films sputtered in Ar and Kr.

Figure 13. Point to point hole resolution vs. film thickness for amorphous Al_2O_3 film exposed with dose of 172×10^2 A/cm^2, 13×10^2 A/cm^2, and 4×10^2 C/cm^2.

Figure 14. Dot patterns produced in amorphous Al_2O_3 film.

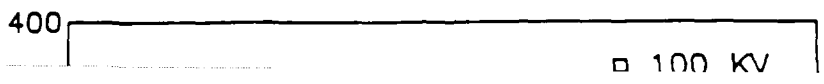

Table 1. Argon concentration in rf sputtered films.

Material	Substrate Temp.(°C)	Film Structure	Argon Concentration (At. %)
Al_2O_3	25	Polycrystalline	< 0.5
	-196	Amorphous	2.41
SiO_2	25	Amorphous	< 0.5
	-196	Amorphous	< 0.5
ZrO_2	25	Polycrystalline	< 0.5
	-196	Amorphous*	2.16
Y_2O_3	25	Polycrystalline	< 0.5
	-196	Amorphous*	0.80
Sc_2O_3	25	Polycrystalline	< 0.5
	-196	Amorphous	3.06
In_2O_3	25	Polycrystalline	< 0.5
	-196	Polycrystalline	< 0.5
$3Al_2O_3 \cdot 2SiO_2$	25	Amorphous	0.85
	-196	Amorphous	1.70
$MgO \cdot Al_2O_3$	25	Amorphous	0.95
	-196	Amorphous	2.58

* These films were difficult to reproduce.

Table 2. E-beam irradiation response in rf sputtered oxide thin film.

Material	Initial Response	Structure Size	Exposure Dose Requirement
Polycrystalline:			
Al_2O_3	none	—	—
Y_2O_3	none	—	—
ZrO_2	none	—	—
Sc_2O_3	none	—	—
In_2O_3	none	—	—
Amorphous:			
Al_2O_3	rapid	5 nm	5×10^3 C/cm^2
Y_2O_3	rapid	5 nm	5×10^3 C/cm^2
$3Al_2O_3 \cdot 2SiO_2$	rapid	5 nm	5×10^3 C/cm^2
$MgO \cdot Al_2O_3$	rapid	10 nm	5×10^3 C/cm^2
Sc_2O_3	rapid	10 nm	5×10^3 C/cm^2
ZrO_2	slow	8 nm	1×10^6 C/cm^2
SiO_2	none	—	—

Table 3. Summary of oxide material properties

Material	Ionic Character (%)	ΔH^{o}_{f} (kJ/mol)	M.P. (°C)
SiO_2	45	-859.4	1713
In_2O_3	49	-930.9	1910
MgO	68	-600.9	2852
ZrO_2	67	-1080.3	2715
Al_2O_3	56	-1669.8	2030
Y_2O_3	70	-1897.9	2410
Sc_2O_3	66	-1902.1	> 2405

Table 4. Inert gas concentration in amorphous Al_2O_3 films.

Sputtering Pressure	Gas	Inert Gas Concentration (At. %)
40 mTorr	Ar	2.41 At. %
60 mTorr	Ar	2.11 At. %
100 mTorr	Ar	1.11 At. %
60 mTorr	Kr	2.15 At. %

Table 5. Center to center hole resolution in amorphous Al_2O_3

Sample Thickness (nm)	Total Dose ($\times 10^2$ C/cm^2) 4	13	43	172
17.5	**	10.3 nm*	11.2 nm	12.9 nm
52.5	**	8.9 nm*	10.3 nm	12.9 nm
87.5	7.4 nm*	8.1 nm*	8.9 nm	8.9 nm
122.5	**	**	12.9 nm	15.2 nm

* material not completely removed
** holes could not be clearly distinguished

Resist Substrate Structure

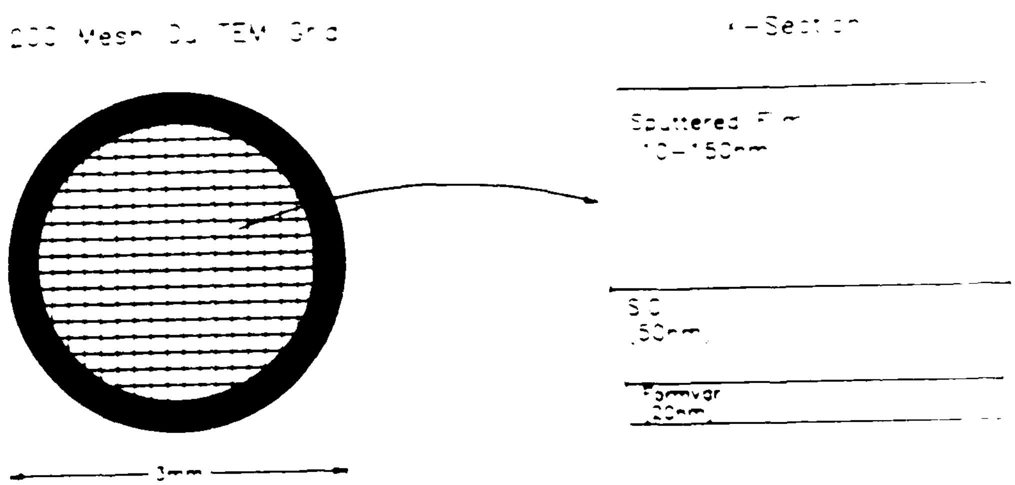

Figure 1 [illegible]

support [illegible] sputtered film [illegible]

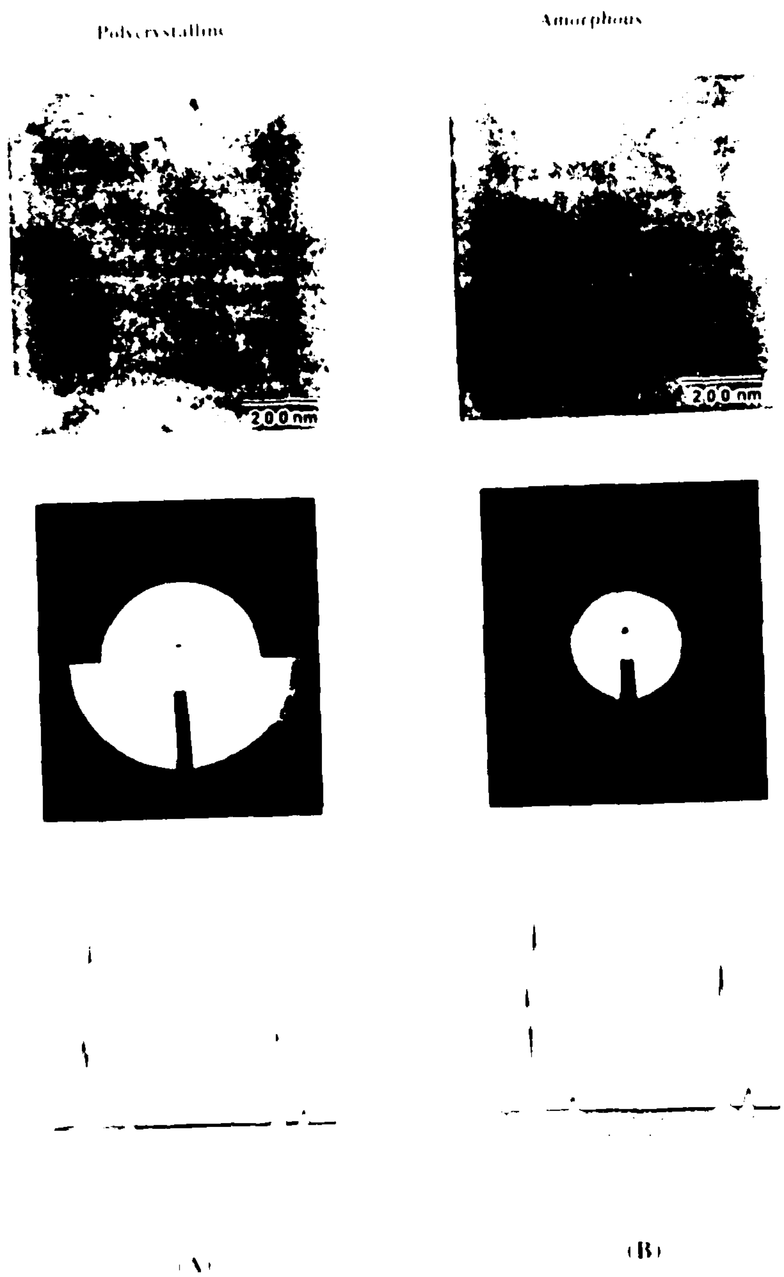

Figure 2. TEM bright field image, corresponding SAD pattern and X-ray spectra of rf sputtered (A) polycrystalline Al_2O_3 and (B) amorphous Al_2O_3 films.

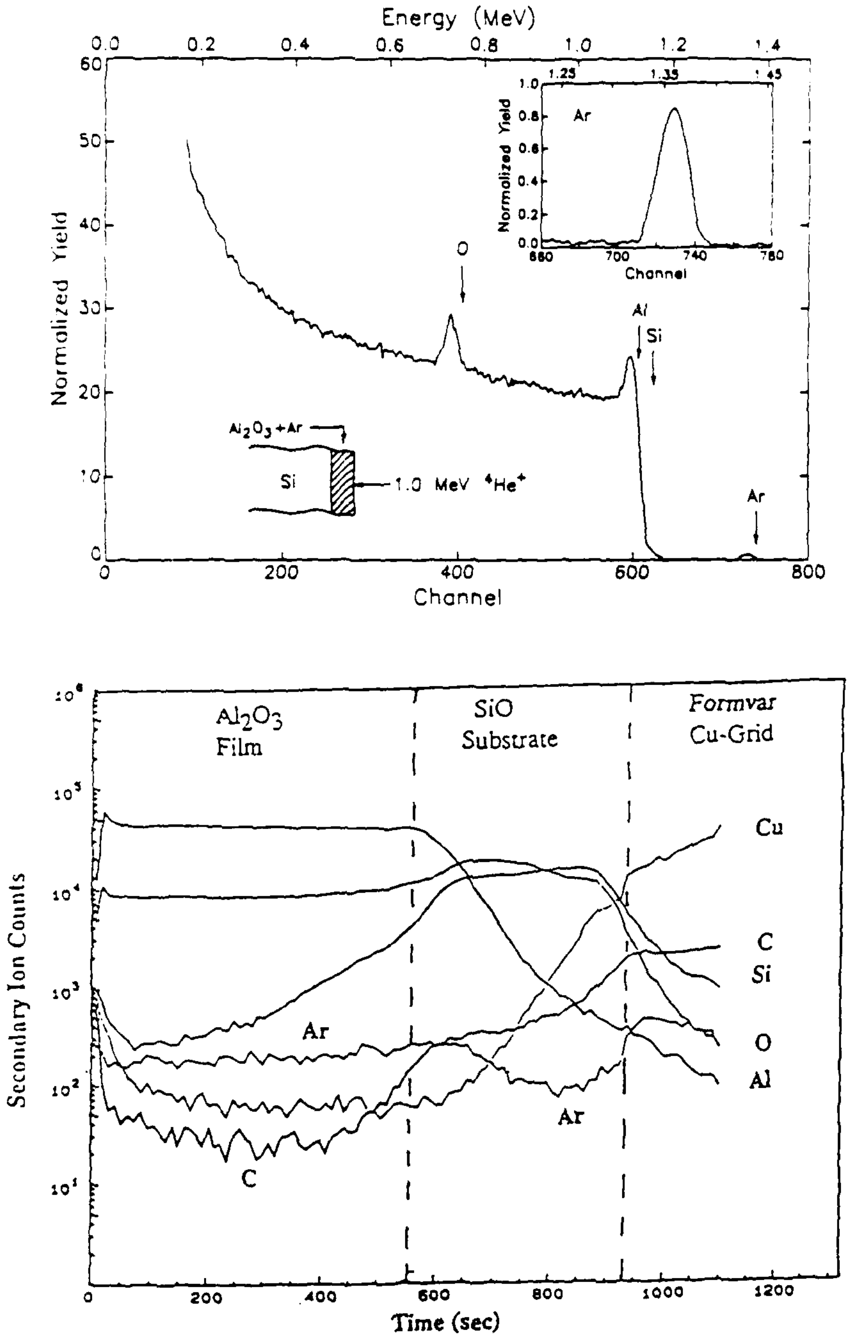

Figure 3. (A) RBS and (B) SIMS spectra from amorphous Al_2O_3 film.

(A)

(B)

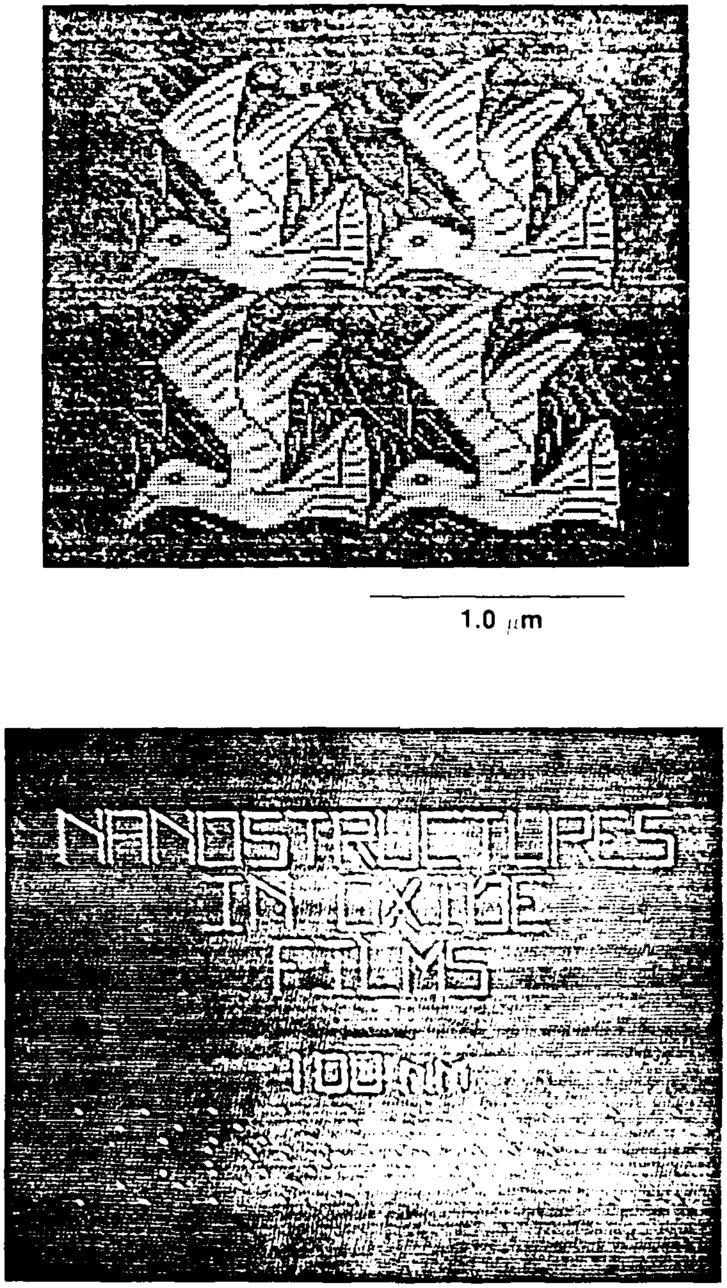

Figure 4. Lithographic structures which have been produced in amorphous films of (A) Al_2O_3 and (B) $3Al_2O_3 \cdot 2SiO_2$ using e-beam irradiation.

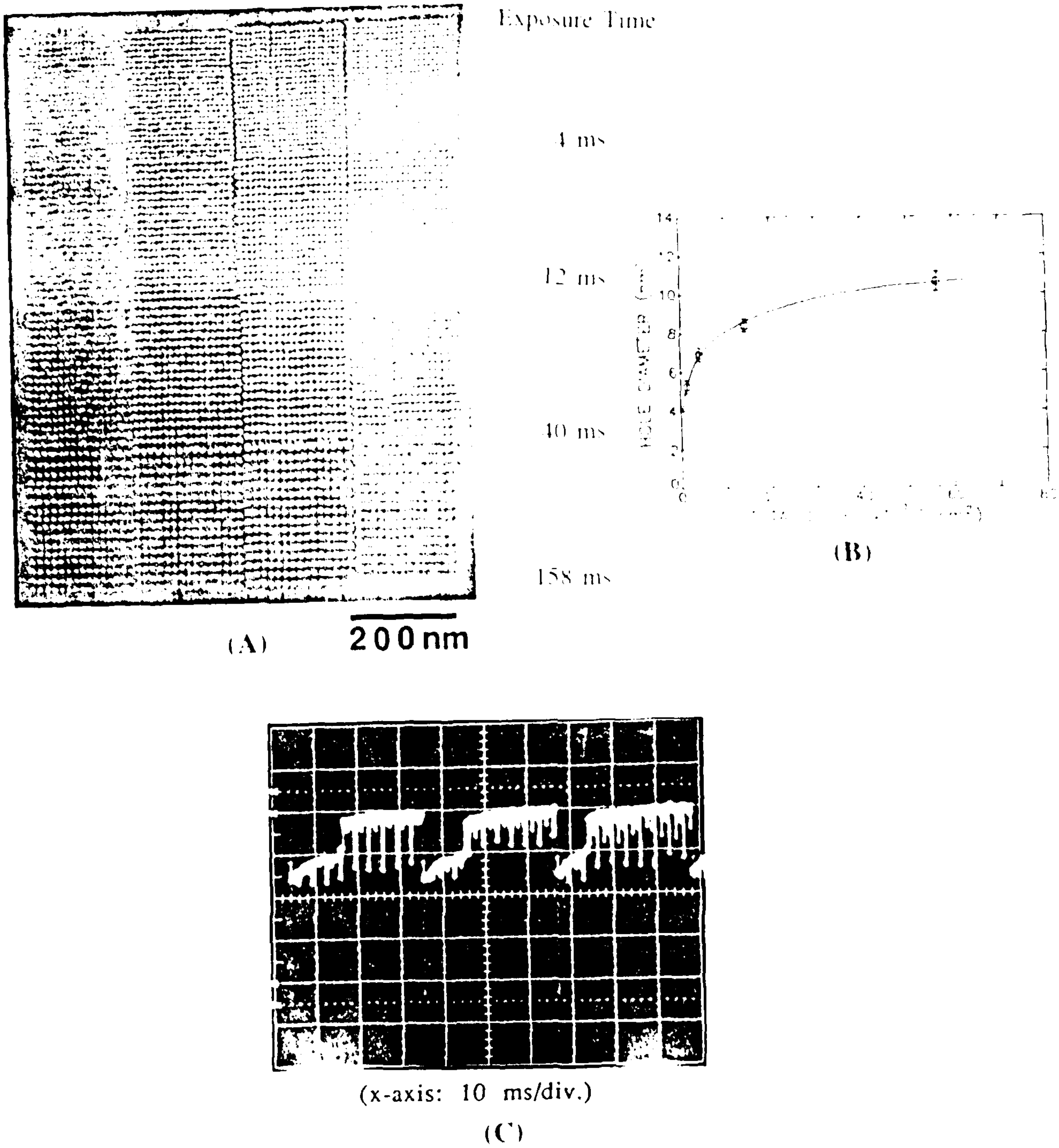

Figure 5. Hole development in an 87.5 nm thick amorphous Al_2O_3 film as indicated by (A) a bright field image of a multiple dose, multiple spacing pattern, (B) the resulting hole diameter as a function of exposure time and (C) the transmitted signal during exposure of three consecutive holes (dose rate 1.08×10^7 A/cm^2)

(A)

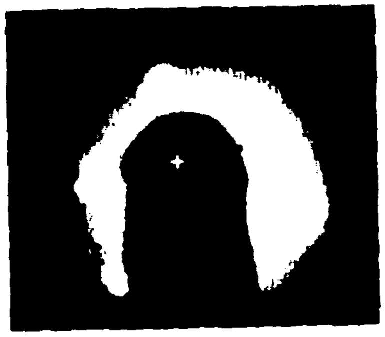

Aluminum: B = [$\bar{1}$11]

(B)

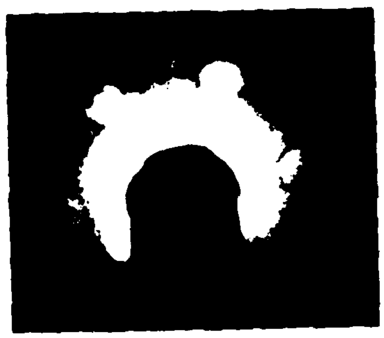

Yttrium: B = [0001]

(C)

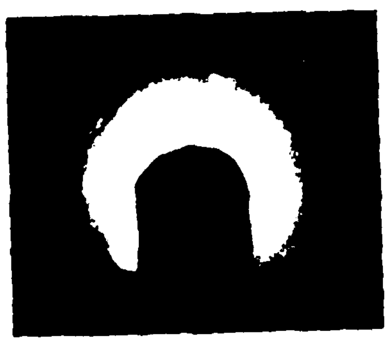

Zirconium: B = [1$\bar{2}$1$\bar{3}$]

Figure 7. Microdiffraction patterns taken from regions near newly created structures in (A) Al_2O_3, (B) Y_2O_3 and (C) ZrO_2 corresponding to patterns of metallic Al, Y and Zr respectively.

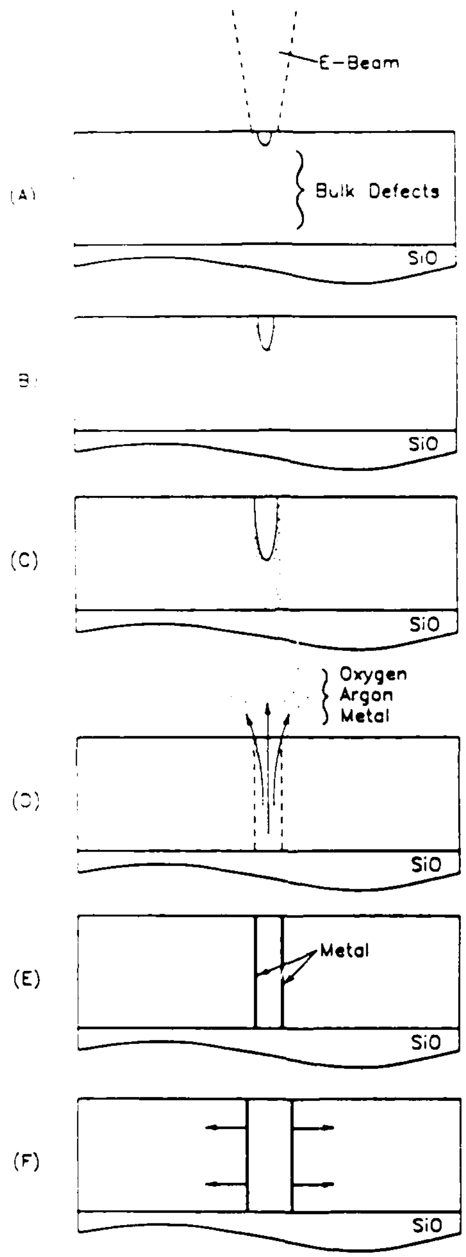

Figure 8. Schematic illustration of material removal process in oxide resists: (A) desorption of surface oxygen and creation of bulk defects, (B) and (C) further surface desorption and defect generation, (D) rapid loss of remaining constituents, (E) Completed hole with metallic species remaining behind and (F) continued increase in hole diameter.

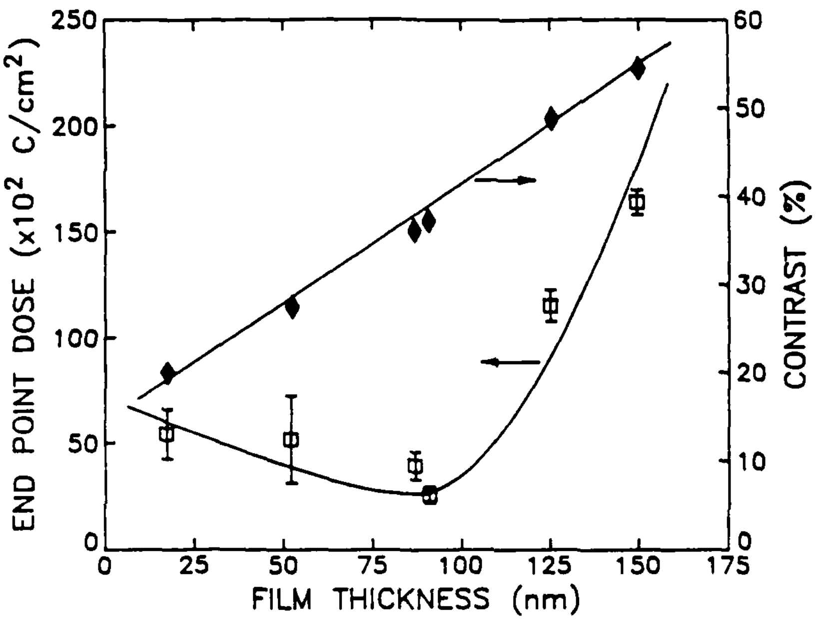

Figure 9. End point dose and contrast measures as a function of film thickness for amorphous Al_2O_3 films.

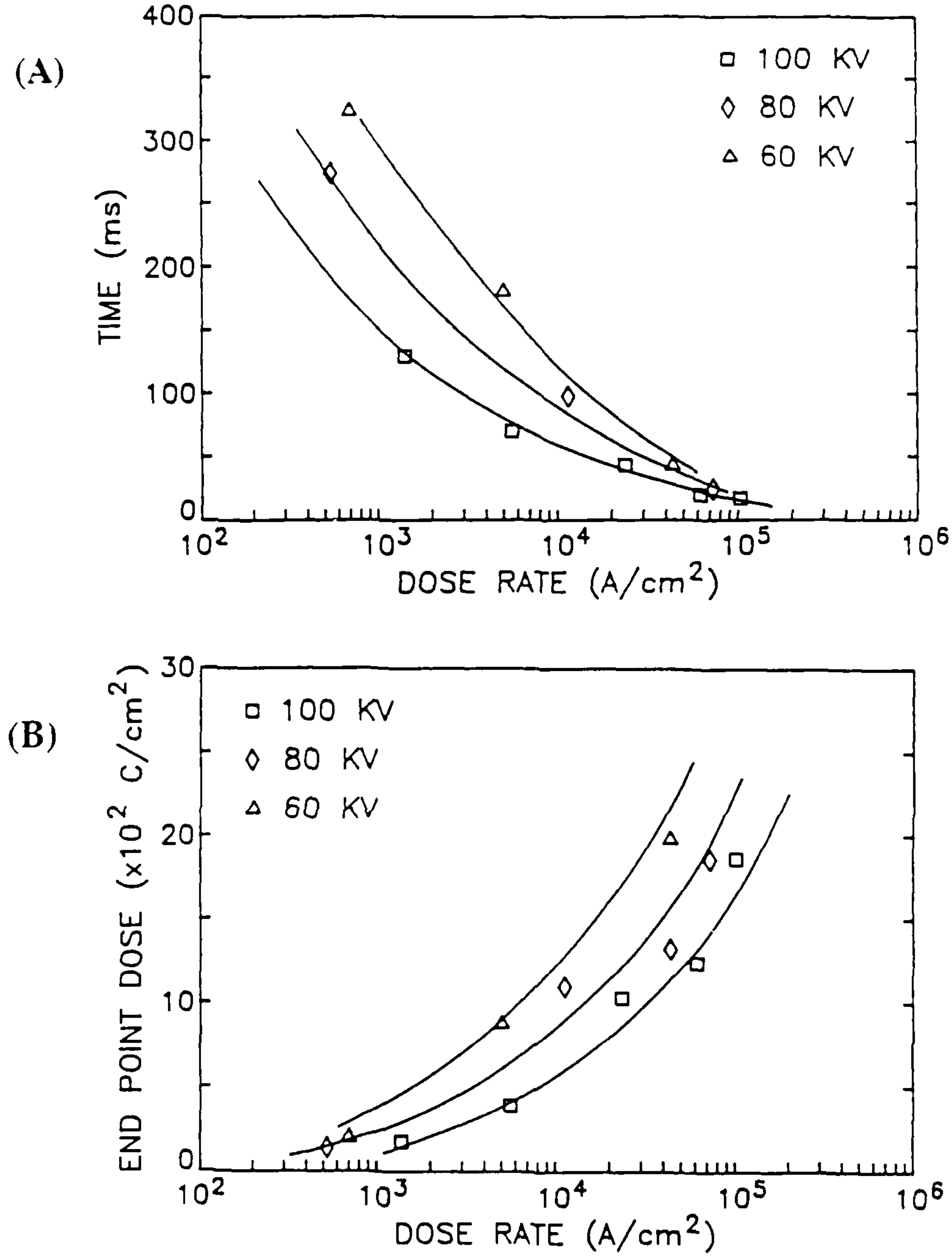

Figure 10. The effect of dose rate and accelerating potential on the (A) time and (B) end point dose required to expose an 87.5 nm thick amorphous Al_2O_3 film.

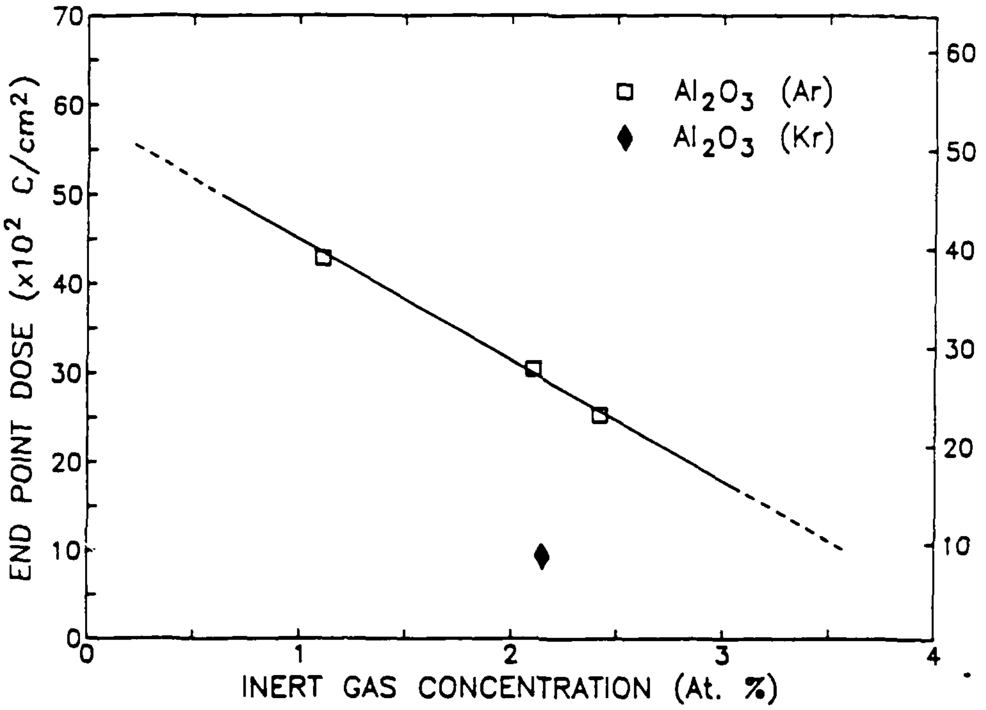

Figure 11. End point dose and exposure time required to expose 90 nm thick amorphous Al_2O_3 film as a function of Ar concentration (dose rate : 1.08×10^5 A/cm^2).

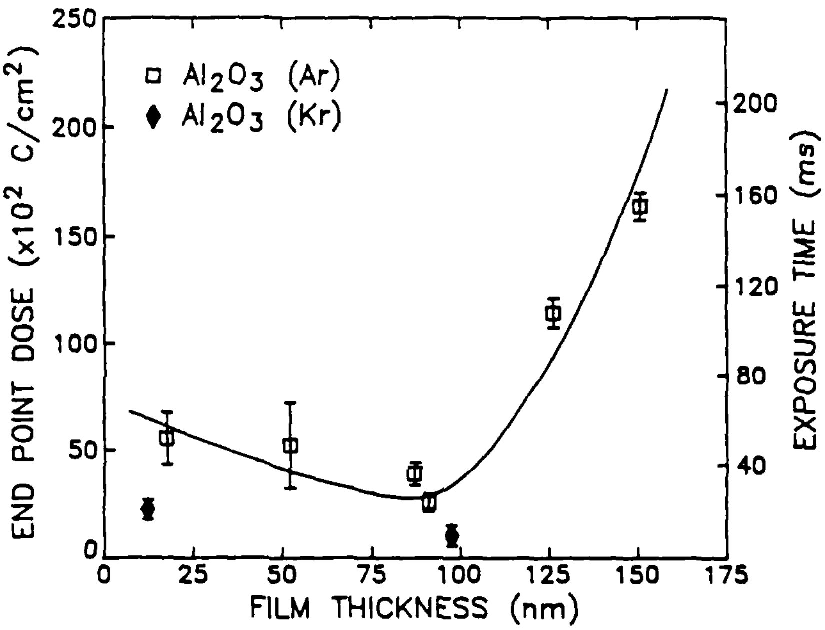

Figure 12. End point dose as a function of film thickness for amorphous Al_2O_3 films sputtered in Ar and Kr.

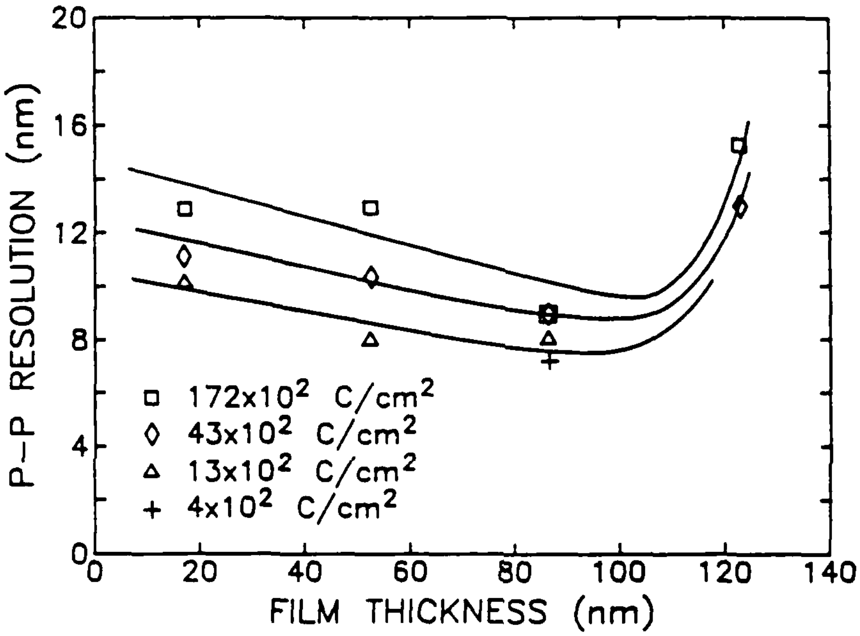

Figure 13. Point to point hole resolution vs. film thickness for amorphous Al_2O_3 film exposed with dose of 172×10^2 A/cm^2, 13×10^2 A/cm^2, and 4×10^2 C/cm^2.

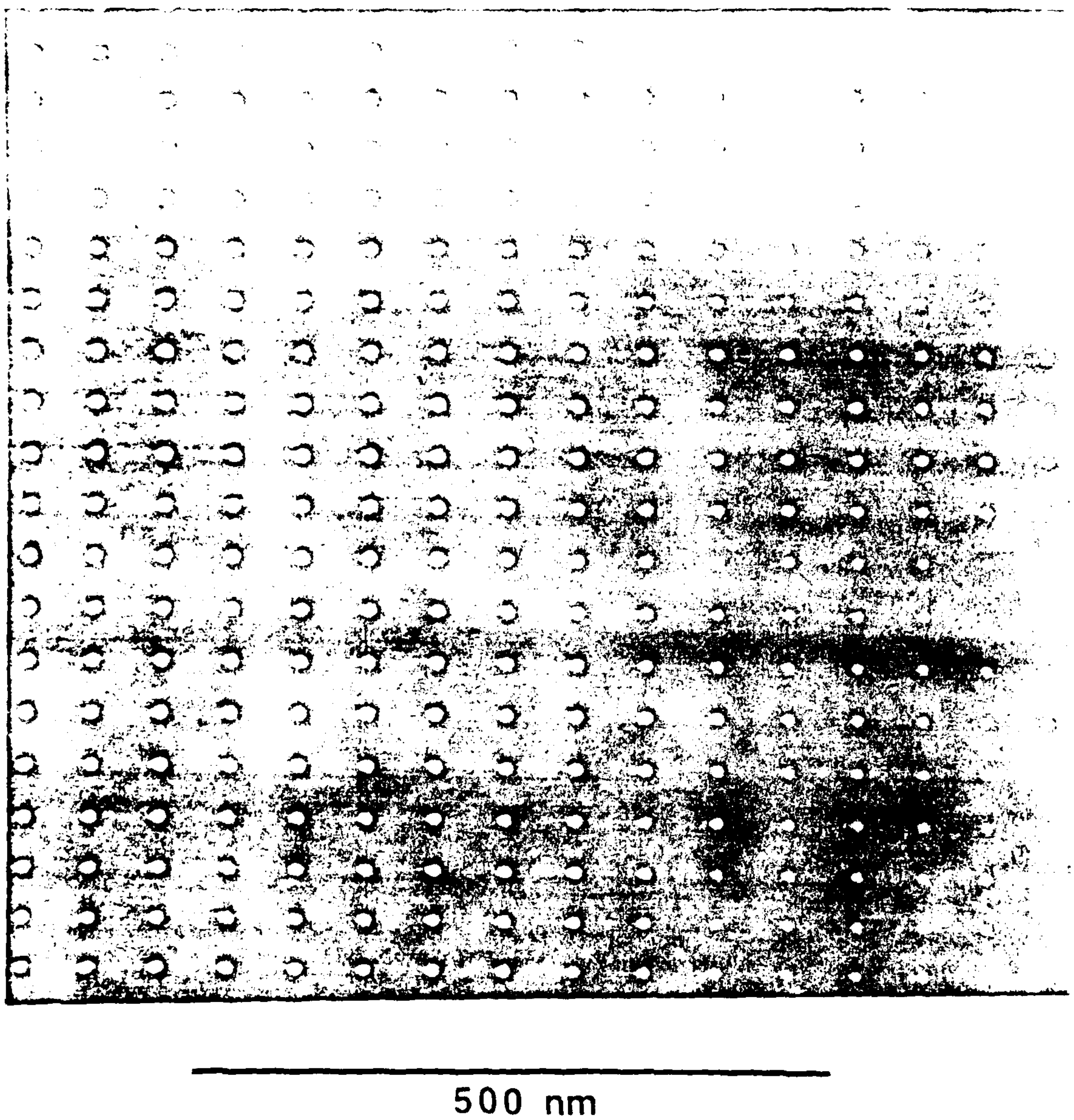
500 nm